An EMG-CT Method Using Multiple Surface Electrodes in the Forearm

Yasuhiro Nakajima[a], Saran Keeratihattayakorn[b], Satoshi Yoshinari[a], Shigeru Tadano[b*]

[a] Industrial Research Institute, Hokkaido Research Organization, Kita 19-jo Nishi 11-chome, Kita-ku, Sapporo, Hokkaido, 060-0819, Japan

[b] Division of Human Mechanical Systems and Design, Faculty of Engineering, Hokkaido University, Kita 13-jo Nishi 8-chome, Kita-ku, Sapporo, Hokkaido, 060-8628, Japan

* Corresponding author:

Shigeru TADANO, PhD

Professor, Division of Human Mechanical Systems and Design, Faculty of Engineering, Hokkaido University

Kita 13-jo Nishi 8-chome, Kita-ku, Sapporo 060-8628, Japan

Tel/Fax: +81-11-7066405, E-mail: tadano@eng.hokudai.ac.jp

Word count: 2771 words (Introduction through Conclusions)

Manuscript Type: Original Article

Key words: Forearm, Surface Electromyography, Muscle Activity, Optimization, Conductive Model.

Abstract

Electromyography computed tomography (EMG-CT) method is proposed for visualizing the individual muscle activities in the human forearm. An EMG conduction model was formulated for reverse-estimation of muscle activities using EMG signals obtained with multi surface electrodes. The optimization process was calculated using sequential quadratic programming by comparing the estimated EMG values from the model with the measured values. The individual muscle activities in the deep region were estimated and used to produce an EMG tomographic image. For validation of the method, isometric contractions of finger muscles were examined for three subjects, applying a flexion load (4.9, 7.4 and 9.8 N) to the proximal interphalangeal joint of the middle finger. EMG signals in the forearm were recorded during the tasks using multiple surface electrodes, which were bound around the subject's forearm. The EMG-CT method illustrates the distribution of muscle activities within the forearm. The change in amplitude and area of activated muscles can be observed. The normalized muscle activities of all three subjects appear to increase monotonically with increases in the load. Kinesiologically, this method was able to estimate individual muscle activation values and could provide a novel tool for studying hand function and development of an examination for evaluating rehabilitation. (200 words)

1. Introduction

The human hand is an excellent end-effector of the upper limb capable of innumerable actions, from fine operations to heavy-duty tasks. A complex movement of the hand is generated by the coordination of many muscles and tendons in the forearm. For best understanding of hand and finger function, individual muscle activity in the forearm must be observable. Electromyography (EMG) has been widely used as a standard tool for studying the kinesiology of muscles. An intramuscular needle electrode is usually employed to detect the activity of deep muscles in the forearm. However, using the needle electrode is a painful procedure and not appropriate for clinical application. Surface electromyography (sEMG) is preferable because of its ease of use and noninvasive nature. The drawback of sEMG is that signals in a region where a large number of muscles lie close together are superimposed (Perry et al., 1981; De Luca and Merletti, 1988; Winter et al., 1994). This superimposition makes observation of individual muscle activities in the forearm difficult, limiting the usefulness of sEMG. A method to overcome this problem would allow accurate observation of individual muscle activity.

In previous attempts to extract motor information from sEMG, the relationship between the muscle action potential (MAP) of a motor unit (MU) and surface conduction has

been established using a scanning EMG method (Stalberg and Antoni, 1980), and the position of the activated single MU in the biceps has been estimated with surface electrodes placed around the upper arm (Roeleveld et al., 1997). The activities of MUs in forearm muscles have been estimated from sEMG signals using an array electrode and blind-deconvolution techniques (Garcia et al., 2005; Yano et al., 2001; Nakamura et al., 2004a; Nakamura et al., 2004b). However, these methods do not work well when many MUs in many muscles are activated at the same time (e.g., in heavy work using the forearm) (Buchthal and Schmalbruch, 1980). Recently, sEMG equipment using a multi-electrode array has been employed (Blok et al., 2002; Merletti et al., 2003) but the analysis of single MU firing patterns and MU characteristics is still complicated and time-consuming (Drost et al., 2006).

The authors have attempted to measure the activity of the individual muscles in the forearm using the reduction characteristics of the sEMG power. Firstly, the reduction characteristics of the sEMG power have been studied. The power exponent of the attenuation (PEA) in relation to the distance between the surface electrode and a source of MAP was calculated using the finite element analysis with a cylindrical conduction model (Nakajima et al., 2008). The position and the activity of the source in the model have been reverse-estimated using an optimization method. Further, the position and the

activity have been also estimated using an experimental phantom-forearm conduction model filled with finely ground specimens of muscle (Kuiken et al., 2001; Nakajima et al., 2009). The source immersed in the model has been estimated from the sEMG power of the surface electrodes.

The purpose of this study was to develop a new EMG technique, the electromyography computed tomography (EMG-CT) method, as a tool for investigating muscle activities in the forearm based on the distribution of sEMG on the skin surface. Muscle activities are calculated by comparing the measured sEMG to simulated results from the mathematical model. The development of EMG-CT will be very useful in studying muscular strategies and mechanisms of muscles in the forearm, which may potentially be used for evaluation of neuromuscular rehabilitation.

2. Methods

2.1 EMG conduction model in the forearm

The muscle region of the forearm was divided into small elements for calculation (Fig. 1). We have formulated the mathematical model relating the mean square value of the MAP (V_{ik}) changes to the PEA *(b)*;

$$\bar{V}_{ik}{}^{2} = V_0(d_i)^2 f_k I_k{}^2 \left(\frac{l_{ik}}{l_0}\right)^{2b(d_i)} \quad (1)$$

where d_i is the distance between the pair of bipolar electrode i (mm), I_k is the strength of the current dipole in muscle fiber k (mA),V_0 is a transformation coefficient (mV/mA), f_k is the firing rate of muscle fiber k, l_{ik} is the conduction distance, and l_0 is the unit length (1 mm). A previous study also showed that V_0 and b are functions of inter electrode distances (IED) of the bipolar electrode d (Fig. 2 and Table 1) (Nakajima et al., 2008).

From the macroscopic point of view, we considered that MUs in any muscles fire independently. Thus, the statistical summation of power of the MAP from each muscle fiber is possible. The muscle activation from all muscle fibers k detected by a bipolar electrode i (V_i) can be simply expressed as

$$\bar{V}_i{}^{2} = \sum_k \bar{V}_{ik}{}^{2} = V_0(d_i)^2 \sum_k f_k I_k{}^2 \left(\frac{l_{ik}}{l_0}\right)^{2b(d_i)} \quad (2)$$

For simplicity, let ${m_k}^2 = f_k {I_k}^2$ be the mean square muscle action current of activated fiber k. The equation can then be rewritten as

$$\bar{V}_i^{\,2} = V_0(d_i)^2 \sum_k {m_k}^2 \left(\frac{l_{ik}}{l_0}\right)^{2b(d_i)} \tag{3}$$

The MAP from element j is a superposition of the contributing action potentials from all the fibers within the element. By summation of all muscle activation of muscle fiber k in element j ($k \in muscle\ j$) gives

$$\bar{V}_i^2 = \sum_j \left\{ V_0(d_i)^2 \sum_{k \in \text{muscle } j} {m_k}^2 \left(\frac{l_{ik}}{l_0}\right)^{2b(d_i)} \right\} = \sum_j \overline{V_{ij}}^2 \tag{4}$$

Here, the mean square muscle action current in muscle element j (m_j^2) can be calculated as

$$m_j{}^2 = \frac{1}{n_j} \sum_{k \in \text{muscle } j} m_k{}^2 \quad (k \in \text{muscle } j) \tag{5}$$

The mean square MAP of element j, $\overline{V_{ij}}^2$ can then be rewritten as

$$\overline{V_{ij}}^2 = V_0(d_i)^2 m_j{}^2 \sum_{k \in \text{muscle } j} \left(\frac{l_{ik}}{l_0}\right)^{2b(d_i)} \tag{6}$$

The mean square sEMG detected by bipolar electrode *i* is considered to be the summation of muscle activation from all elements *j*. Letting L_{ij} be the transfer coefficient simplifies the equation to

$$\overline{V_i}^2 = \sum_j \overline{V_{ij}}^2 = \sum_j L_{ij} m_j{}^2 \tag{7}$$

where

$$L_{ij} = V_0(d_i)^2 \sum_{k \in \text{muscle } j} \left(\frac{l_{ik}}{l_0}\right)^{2b(d_i)} \tag{8}$$

The sEMG signal from each bipolar electrode pair can be calculated from the EMG conduction model described above.

2.2 Muscle elements

In this study, the division of the muscle element region was performed by Voronoi tessellation. The base points of muscle elements were placed using the finite element algorithm. The set of seeds was distributed across the circular region with an element size of 1 mm for the surface region and 4 mm for the inside region.

2.3 Optimization process

To estimate the muscle activation of each muscle element, sequential quadratic programming (SQP) was used to optimize the value (Fig. 3). SQP is generally used to solve non-linear equations. The objective function f is given by

$$f = \sum_{i} (V_i - V_{\mathrm{M}i})^2 \tag{9}$$

where V_i is the calculated sEMG from equation 7 and V_{Mi} is the measured sEMG from the experiment. The search direction in which the gradient ∇f of the objective function vanishes can be expressed as the function

$$\min_{[D_j]} \left\{ \nabla f^T [D_j] + \frac{1}{2} [D_j]^T \nabla^2 f [D_j] \right\} \tag{10}$$

where D_j is the search direction. The optimization was calculated using the Optimization Toolbox in MATLAB (Mathswork, USA).

2.4 Muscle arrangement in forearm

To quantify each muscle activity, it was necessary to determine the location of each muscle in the cross-sectional area. The arrangement of muscles in the forearm was reconstructed by tracing the muscle boundary from an MR image of each subject [Fig. 4(a)]. Thirteen muscles were traced for each forearm [Fig. 4(b)]: the e*xtensor carpi ulnaris* (ECU), e*xtensor digiti minimi* (EDM), *extensor digitorum communis* (EDC), *extensor pollicis longus* (EPL), *abductor pollicis longus* (APL), *extensor carpi radialis*

longus (ECRL), *extensor carpi radialis brevis* (ECRB), *flexor digitorum profundus* (FDP), *flexor pollicis longus* (FPL), *brachioradialis* (BR), *flexor carpi ulnaris* (FCU), *flexor digitorum superficialis* (FDS), and *flexor carpi radialis* (FCR).

2.5 Subjects

Three right-handed male subjects participated in this study (age: 35.3 ± 2.4 years; height: 175.3 ± 3.4 cm; body mass: 64.7 ± 4.6 kg; mean ± SD). None of the participants had a history of trauma affecting the upper limbs. The thickness of subcutaneous fat and skin were measured with a skinfold caliper. The procedures were approved by the Ethical Review Board for the Protection of Persons in Biomedical Research, Graduate School of Engineering, Hokkaido University, and all subjects signed an informed consent agreement.

2.6 Experimental procedures

The subjects sat on a chair with their forearm placed on a horizontal table. The upper arm was at 0° of abduction, the elbow joint flexed at 90° and the wrist was placed in supinated position. The wrist, palm, and proximal phalanx of the middle finger were

fixed to the table [Fig. 5(a)]. A weight was hung on the middle phalanx of the middle finger with a cotton thread; at a position 10 mm distal from the proximal interphalangeal (PIP) joint [Fig. 5(b)]. The load was applied for 5 seconds and repeated thrice with 5-second rest intervals. The weights of the load were 0.50, 0.75, and 1.00 kg. The loads were selected to be 10-20% of maximal finger tip force (50N), since they do not cause muscle fatigue.

2.7 Surface EMG set-up and data acquisition

The sEMG signals from the forearm were recorded with 20 custom-built electrode plates. The electrode plate comprised four aligned 3 mm diameter disciform stainless steel electrodes (Fig. 6). IED of the differential bipolar electrodes were 15 and 45 mm, with the middle points coinciding. sEMG recording using a bipolar electrode with wide IED can detect distant muscle activation because of low attenuation (Nakajima et al., 2008), whereas a bipolar electrode with narrow IED can detect activation only at short distances. Bipolar electrode pairs can detect muscle activation at different depths.

The electrode plates were bound around the subject's forearm, with the middle point at 1/3 of the forearm length from the *radial styloid process*, parallel to the axis of the

radius. Before binding the electrode plates, their forearm skin was shaved by a razor and cleansed by alcohol swab; the electrodes were pasted with conductive gel. The sEMG signals were obtained with a custom-built amplifier connected to the electrodes with a >1GΩ input impedance, a >100dB common mode rejection ratio (CMRR) and a <100nV/$\sqrt{\text{Hz}}$ signal noise ratio (SNR). The sEMG signals were processed with the amplifier: (1) amplified 1000 times; (2) filtered using fourth-order Butterworth high-pass filter with a 10-Hz cutoff frequency and low-pass filter with a 300-Hz; (3) A/D-converted and recorded on a PC with a sampling rate of 2 kHz/channel using 16-bit, ±10V input range A/D converter (ADA16-32/2(CB)F, CONTEC Co., Ltd. JAPAN). The recorded signals were filtered in the PC using 7th-order Butterworth high-pass digital filter with a 10-Hz cutoff frequency and low-pass digital-filter with a 200-Hz. The root mean square (RMS) value and mean power of each channel were calculated from the recorded signals in 500 ms windows.

3. Results

Figure 7 shows the EMG tomography results for all subjects. The muscular activity of each element was estimated by inverse calculation. The results show the position of active muscle during the contraction. It can be seen that the muscle activities are

unevenly distributed, with the positions of activated muscle consistent with the position of the muscle area from MRI. High muscle activities were found in the FDS and EDC areas. The area and intensity of the high-amplitude region in the tomographic image increased with load. Coactivation of the FDS and EDC areas when a load was applied to the PIP joint is apparent. A flexion load to the PIP joint of the middle finger caused activation of the FDS muscle, reflected in the estimation results. The total muscle activity S_m is defined as the summation of muscle action current (m_j) within the forearm area calculated by

$$S_m = \sum_j (m_j \times A_j) \tag{11}$$

where A_j is the area of element j. Figure 8 shows the total muscle activities of all three subjects, which appear to increase monotonically with load.

4. Discussion

To our knowledge, this is the first study estimating EMG-CT in the human forearm using a multi-surface electrode, providing a new view in EMG studies. The muscle activity of each element was computed from the sEMG signals detected from the skin surface of the forearm. A novelty of this method is that the active muscle area can be located non-invasively during contraction.

Physical experiments were performed to verify the results. The positions of active muscle (Fig. 7) were validated by comparing the area of active elements with the outlines of muscle area [Fig.4(b)]. The activations of muscle are of the FDS, FDP and EDC, which are the primary flexor and extensor of the fingers. Many studies which used intramuscular electrodes to detect muscle activity confirmed that during finger flexion, these muscles were active (Johanson et al., 1990; Maier et al., 1995; Butler et al., 2005). In addition, when load increases from 4.9 N to 9.8 N, the mean of total muscle activity of all subjects increase from 437.6 mADipole/s to 595.6 mADipole/s (Fig. 8). It seems that EMG-CT can investigate muscle activities in the forearm properly.

Muscle activation pattern of Subject 1 and Subject 2 seem to be similar. Both subjects used the same muscle, i.e., the FDS, FDP and EDC to generate muscle force when a

load was applied to the middle finger. The slight different in the activation area and amplitude might due to the different in individual muscle structure. It is noted that Subject 3 seems to use a bit more of the FCR, this might cause by unintentional movement of wrist during the task.

The forearm conduction model used in reverse estimation considered only muscle tissue to reduce the computational load. However, a real forearm contains subcutaneous fat and skin. Lowery et al. (2004) have reported the influence of subcutaneous fat and skin on the crosstalk of the myoelectric potential, using a cylindrical conduction model consisting of muscle tissue, bone, and subcutaneous fat and skin. They concluded that increases in the thickness of subcutaneous fat causes increases in crosstalk. The estimation method proposed in this paper is essentially an analysis of crosstalk. Thus, it may be possible that subcutaneous fat affects estimation. Given that the thickness of subcutaneous fat in the forearm of the subjects was less than 3 mm, its influence on the estimates may be small. However, this factor must be considered during the estimation of deep muscles that generate weak sEMG signals.

Subcutaneous fat also decreases the mean power frequency of the sEMG spectrum, similarly to a low-pass filter, because of the permittivity of the fat (Stoykov et al., 2002). The low-pass filter effect is also caused by the spatial dispersion of the sEMG

distribution (Lindström et al., 1977). The effect is stronger with increased distance between an activated muscle fiber and the surface, and therefore the sEMG power at high frequency is readily reduced. The influence of the low-pass filter effect on reverse estimation may be effectively avoided by use of only the low-frequency components of sEMG for calculation.

The anisotropic conductivity of muscle tissue and muscle alignment from previous studies was used in estimation (Burger and van Dongen, 1961; Schwan and Li, 1953; Geddes and Baker, 1967; Faes et al., 1999; Gabriel et al., 1996). However, in actual measurements, these parameters may be highly dependent on the individual being measured. Increased precision of the estimates requires calibration of these parameters for each subject. Electrical impedance tomography (EIT) can measure the conductivity distribution in the forearm (Cheney et al., 1999). EIT is a method of reconstructing the conductivity distribution in a volume conductor from the electrical potential distribution of the surface caused by the current through the surface electrodes around the conductor. The current is loaded through a pair of the electrodes and potentials are simultaneously measured at other electrodes. The operation is then repeated at all of the electrodes. The conductivity distribution is reconstructed to compare the measured to the simulated potential distributions using finite-element model and an optimization

method. Given that the alignment of electrodes in EIT is approximately that of the estimates, it is useful to measure the conductivity distribution sequentially in an experiment.

The surface electrode position on the forearm should also be calibrated. The estimation method is sensitive to the circumferential electrode positions because many of the muscles in the forearm are thin. The positions will certainly be misaligned even if extreme caution is taken. Thus, it would be impractical to assume high measurement accuracy. For calibrating the electrode position, detection of the electrodes closest to activated index muscles is useful. First, the analyst should activate an index muscle. Then the electrode detecting the strongest sEMG signal can be assumed to be the closest to the activated muscle. Repeated detection using index muscles, will reveal the correct alignment of the electrode.

We have demonstrated that EMG-CT allows the investigation of each muscle activities within the forearm. This method makes possible the noninvasive localization of activated muscle area from the skin surface. It opens a new window on EMG study of the forearm that has potential use in studying muscle mechanisms and as a diagnostic tool for rehabilitation evaluation.

Conflict of interest statement

The authors have no personal or financial conflicts of interest related to publication of the present work.

References

Blok JH, van Dijk JP, Drost G, Zwarts MJ, Stegemean DF. A high-density multichannel surface electromyography system for the characterization of single motor units. Review of Scientific Instruments 2002; 73(4): 1887-97.

Buchthal F, Schmalbruch H. Motor unit of mammalian muscle. Physiological Reviews 1980; 60: 90-142.

Burger HC, van Dongen R. Specific electric resistance of body tissues. Physics in Medicine and Biology 1961; 5:431–47.

Butler TJ, Kilbreath SL, Gorman RB, Gandevia SC. Selective recruitment of single motor units in human flexor digitorum superficialis muscle during flexion of individual fingers. Journal of Physiology 2005; 567.1: 301-309

Cheney M, Isaacson D, Newell JC. Electrical impedance tomography. SIAM Review 1999; 41:85-101.

De Luca CJ, Merletti R. Surface myoelectric signal crosstalk among muscles of the leg. Electroencephalography and Clinical Neurophysiology 1988; 69:568-75.

Drost G, Stegeman DF, van Engelen BG, Zwarts M. Clinical applications of high-density surface EMG: a systematic review. Journal of Electromyography and Kinesiology 2006; 16(6): 586-602.

Faes TJC, van der Meij HA, de Munck JC, Heethaar RM. The electric resistivity of human tissues (100Hz–10MHz): A meta-analysis of review studies. Physiological Measurement 1999; 20: R1-R10.

Gabriel S, Lau RW, Gabriel C. The dielectric properties of biological tissues: II. Measurements in the frequency range 10Hz to 20GHz. Physics in Medicine and Biology 1996; 41: 2251-69.

García GA, Okuno R, Akazawa K. A decomposition algorithm for surface electrode-array electromyogram. IEEE Engineering in Medicine and Biology 2005; 24: 63–72.

Geddes LA, Baker LE. The specific resistance of biological material—a compendium of data for the biomedical engineer and physiologist. Medical and Biological Engineering and Computing 1967; 5: 271-93.

Johanson ME, Skinner SR, Lamoreux LW. St. Helen R, Moran SA, Ashley RK. Phasic relationships of the extrinsic muscles of the normal hand. Journal of Hand Surgery 1990; 15A: 587-594.

Kuiken TA, Stoykov NS, Popović M, Lowery M, Taflove A. Finite element modeling of electromagnetic signal propagation in a phantom arm. IEEE Transactions on Neural Systems and Rehabilitation Engineering 2001; 9(4): 346-54.

Lindström L, Magnusson R. Interpretation of myoelectric power spectra: a model and its applications. Proceedings of the IEEE 1977; 65: 653-62.

Lowery MM, Stoykov NS, Kuiken TA. A simulation study to examine the use of cross-correlation as an estimate of surface EMG cross talk. Journal of Applied Physiology 2004; 94: 1324-34.

Maier MA and Hepp-Reymond MC. EMG activation patterns during force production in precision grip. I. Contribution of 15 finger muscles to isometric force. Exp Brain 1995; 103(1): 108-122.

Merletti R, Farina D, Gazzoni M. The linear electrode array: a useful tool with many applications. Journal of Electromyography and Kinesiology 2003; 13(1): 37-47.

Nakajima Y, Yoshinari S, Tadano S. Surface conduction analysis of EMG signal from forearm muscles. Proceedings of 13th International Congress on Biological and Medical Engineering 2008: 1904–07.

Nakajima Y, Yoshinari S, Tadano S. An experimental model on the activity of forearm muscles using surface electromyography. Journal of Biomechanical Science and Engineering 2009; 4: 212-20.

Nakamura H, Yoshida M, Kotani M, Akazawa K, Moritani T. The application of independent component analysis to the multi-channel surface electromyographic signals for separation of motor unit action potential trains: part I—measuring techniques. Journal of Electromyography and Kinesiology 2004; 14: 423–32.

Nakamura H, Yoshida M, Kotani M, Akazawa K, Moritani T. The application of independent component analysis to the multi-channel surface electromyographic signals for separation of motor unit action potential trains: part II—modeling interpretation. Journal of Electromyography and Kinesiology 2004; 14: 433–41.

Perry J, Easterday CS, Antonelli DJ. Surface versus intramuscular electrodes for EMG of superficial and deep muscles. Physical Therapy 1981; 61: 7-15.

Roeleveld K, Stegeman DF, Vingerhoets HM, van Oosterom A. The motor unit potential distribution over the skin surface and its use in estimating the motor unit location. Acta Physiologica Scandinavica 1997; 161: 465-72.

Schwan HP, Li K. Capacity and conductivity of body tissues at ultrahigh frequencies. Proceedings of the Institute of Radio Engineers 1953; 41: 1735-40.

Stålberg E, Antoni L. Electrophysiological cross section of the motor unit. Journal of Neurology, Neurosurgery and Psychiatry 1980; 43: 469-74.

Stoykov NS, Lowery MM, Taflove A, Kuiken TA. Frequency- and time-domain FEM models of EMG: capacitive effects and aspects of dispersion. IEEE Transactions on Biomedical Engineering 2002; 49: 763-72.

Winter DA, Fuglevand AJ, Archer SE. Crosstalk in surface electromyography: Theoretical and practical estimates. Journal of Electromyography and Kinesiology 1994; 4: 15-26.

Yano H, Fujiwara Y, Maekawa S, Kozima H, Yoshimoto H. Research on Communication Mechanism of Embodied Interaction. NICT Journal 2001; 48(3): 9-20.

Figures Captions

Figure 1 Representation of electromyography conduction model for calculation. Virtual muscle fiber *k* is a part of the muscle element *j*. l_{ik} is the distance between the muscle fiber *k* and the bipolar electrode *i*. V_{ik} is the surface electromyography (sEMG) from muscle fiber k detected by a bipolar electrode.

Figure 2 Power exponent of attenuation (PEA) of the coefficient resulting from the difference in inter-electrode distance (IED) (Nakajima et al., 2008). The strength of surface electromyography is affected by IED of the bipolar electrode.

Figure 3 Optimization process for estimating muscle activity. Calculated and experimentally measured surface electromyography activities were compared. Sequential quadratic programming (SQP) was used to optimize the value.

Figure 4 a) MR image of cross-section of a right forearm b) The arrangement of muscles in the forearm trace from the cross-sectional area of MR image at 1/3 forearm length from the *processus styloideus radii*, palm up. There are thirteen muscles in the cross section: the e*xtensor carpi ulnaris* (ECU), e*xtensor digiti minimi* (EDM), *extensor*

digitorum communis (EDC), *extensor pollicis longus* (EPL), *abductor pollicis longus* (APL), *extensor carpi radialis longus* (ECRL), *extensor carpi radialis brevis* (ECRB), *flexor digitorum profundus* (FDP), *flexor pollicis longus* (FPL), *brachioradialis* (BR), *flexor carpi ulnaris* (FCU), *flexor digitorum superficialis* (FDS), and *flexor carpi radialis* (FCR).

Figure 5 a) Arm posture during testing. The upper right arm of a subject was at 0° of abduction, the elbow joint flexed at 90° and the wrist placed at 0° of flexion, palm up. A total of 40 bipolar electrode pairs were placed around the forearm, with the middle points at 1/3 of the forearm length from the *radial styloid process*, parallel and in the axis of the *radius*. b) A weight was suspended with cotton thread from the middle phalanx of the middle finger, 10 mm from the proximal interphalangeal joint.

Figure 6 Schematic diagram of the electrode plate on which two bipolar electrode pairs were constructed. A pair of electrodes is connected to a differential pre-amplifier.

Figure 7 Electromyography computed tomography of all subjects when the flexion load (4.9, 7.4 and 9.8 N) was applied to the proximal interphalangeal joint of the middle phalanx.

Figure 8 The relationship between the total muscle activation within forearm and load applied to the proximal interphalangeal joint of the middle phalanx of all subjects.

Figure 1

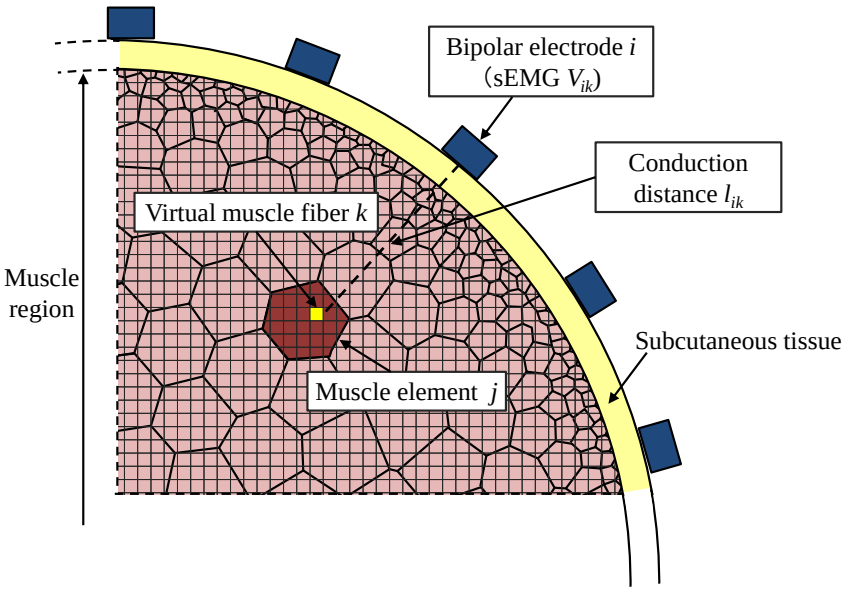
Bipolar electrode i
(sEMG V_{ik})
Conduction distance l_{ik}
Virtual muscle fiber k
Muscle region
Subcutaneous tissue
Muscle element j

Figure 2

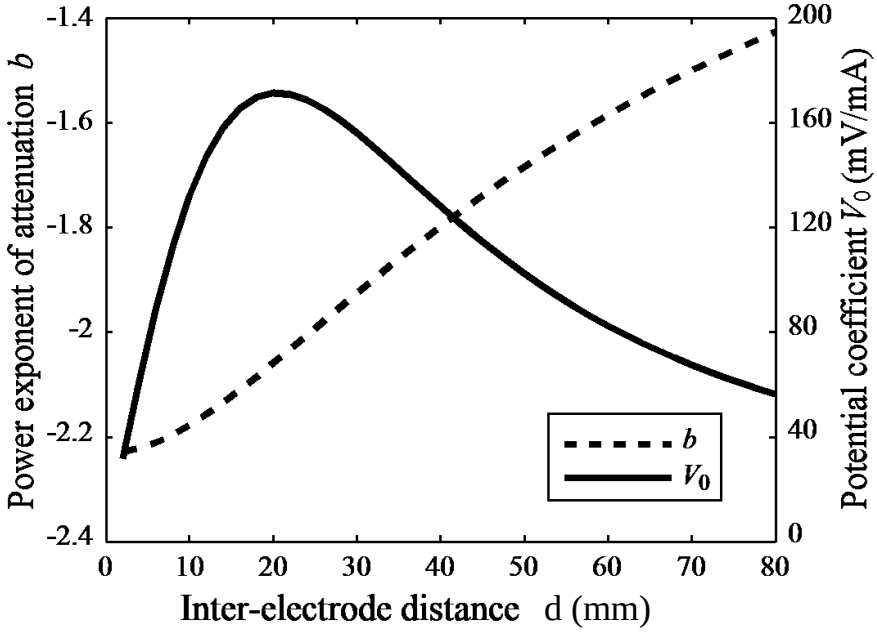
-1.4
-1.6
-1.8
-2
-2.2
-2.4
Power exponent of attenuation b
200
160
120
80
40
0
Potential coefficient V0 (mV/mA)
0
10
20
30
40
50
60
70
80
Inter-electrode distance d (mm)
b
V0

Figure 3

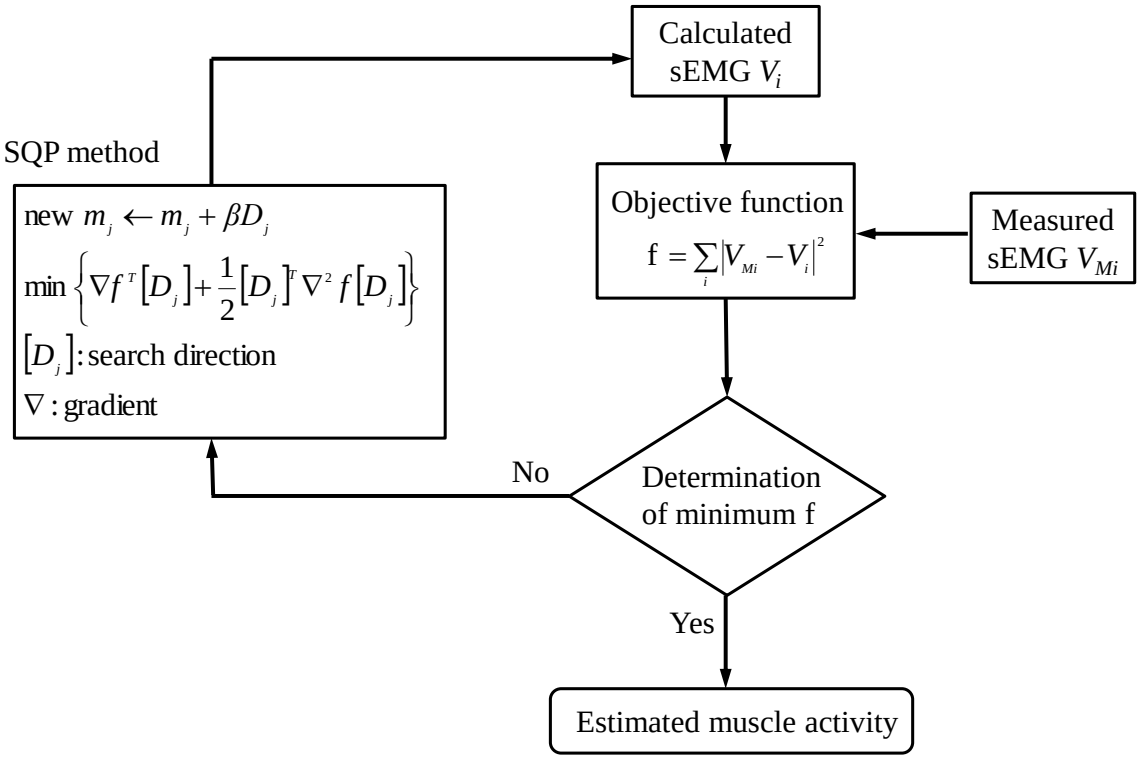
Calculated sEMG V_i
SQP method
new $m_j \leftarrow m_j + \beta D_j$
$\min\left\{\nabla f^T[D_j] + \frac{1}{2}[D_j]^T \nabla^2 f[D_j]\right\}$
$[D_j]$: search direction
∇ : gradient
Objective function
$f = \sum_i |V_{Mi} - V_i|^2$
Measured sEMG V_{Mi}
No
Determination of minimum f
Yes
Estimated muscle activity

Figure 4

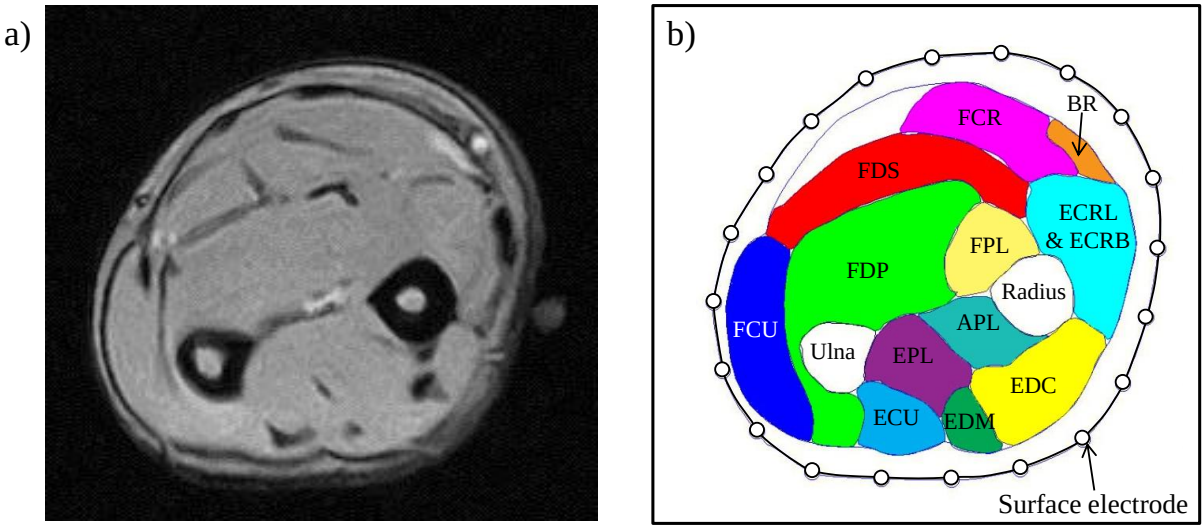
a)
b)
FCR
BR
FDS
ECRL
& ECRB
FPL
FDP
Radius
APL
FCU
Ulna
EPL
EDC
ECU
EDM
Surface electrode

Figure 5

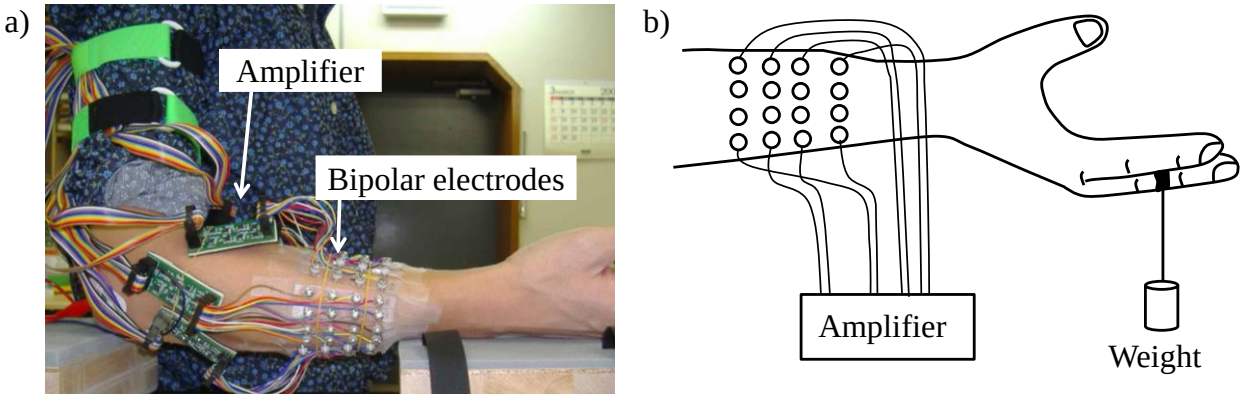

Figure 6

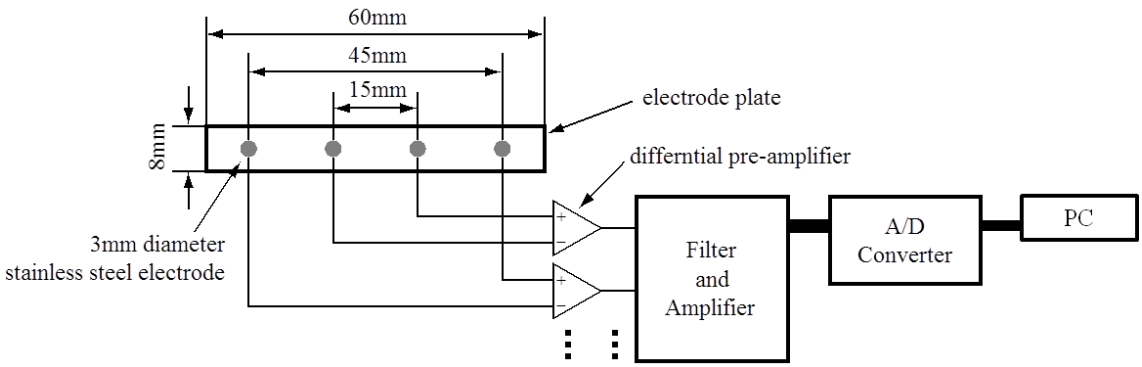
60mm
45mm
15mm
8mm
electrode plate
differntial pre-amplifier
3mm diameter
stainless steel electrode
Filter
and
Amplifier
A/D
Converter
PC

Figure 7

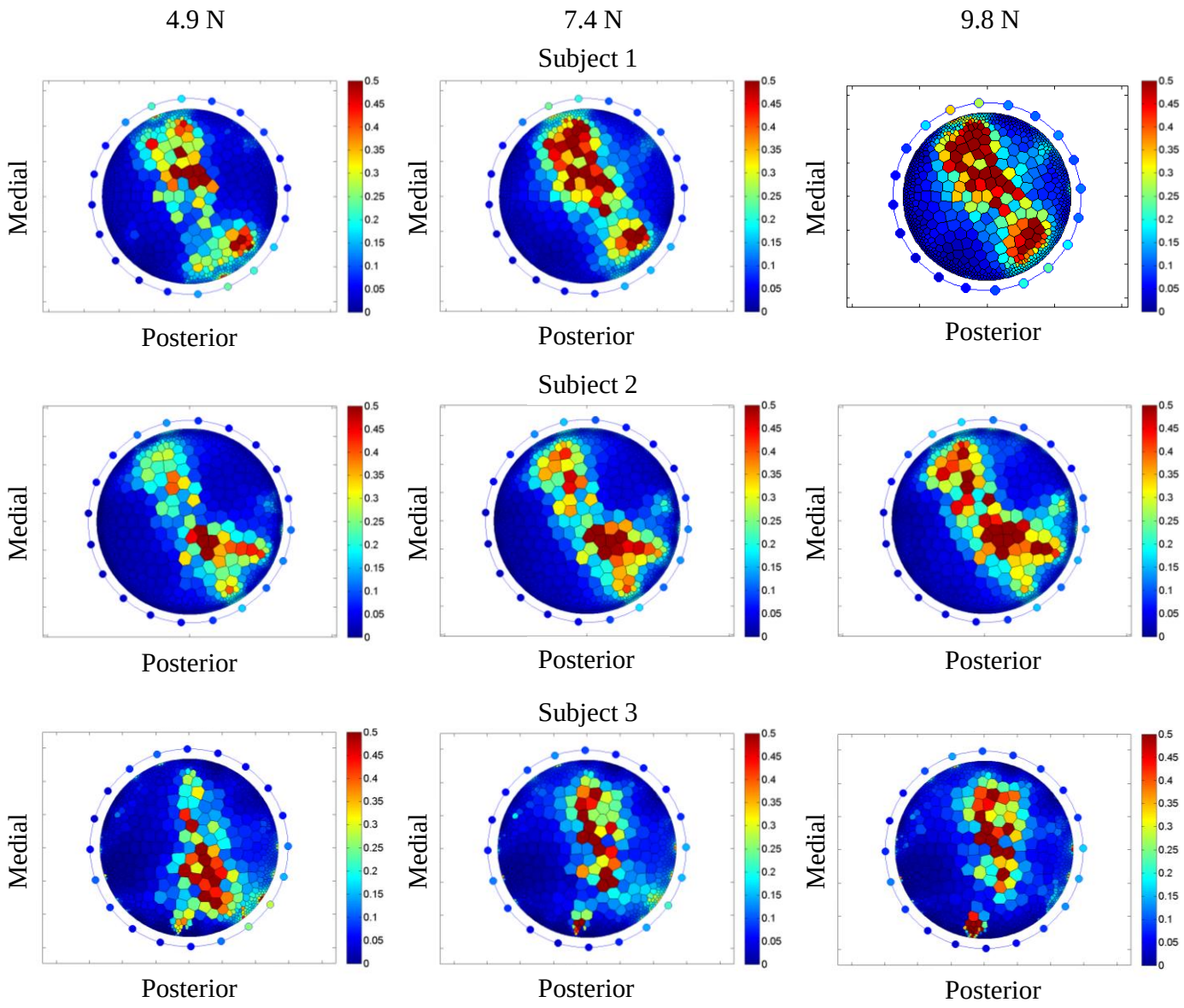
4.9 N
7.4 N
9.8 N
Subject 1
Subject 2
Subject 3
Medial
Posterior
0.5
0.45
0.4
0.35
0.3
0.25
0.2
0.15
0.1
0.05
0

Figure 8

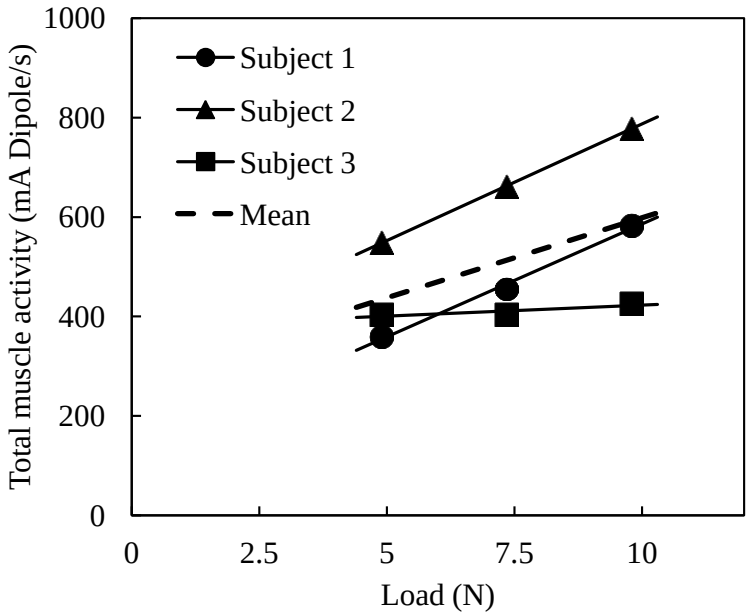
1000
800
600
400
200
0
Total muscle activity (mA Dipole/s)
Subject 1
Subject 2
Subject 3
Mean
0
2.5
5
7.5
10
Load (N)